

# Exotic phase diagram of a cluster charging model of bosons on the kagome lattice

Sergei V. Isakov,<sup>1</sup> Arun Paramekanti,<sup>1</sup> and Yong Baek Kim<sup>1,2</sup>

<sup>1</sup>*Department of Physics, University of Toronto, Toronto, Ontario M5S 1A7, Canada*

<sup>2</sup>*School of Physics, Korea Institute for Advanced Study, Seoul 130-722, Korea*

(Dated: October 26, 2018)

We study a model of hard-core bosons on the kagome lattice with short-range hopping ( $t$ ) and repulsive interactions ( $V$ ). This model directly maps on to an easy-axis  $S = 1/2$  XXZ model on the kagome lattice and is also related, at large  $V/t$ , to a quantum dimer model on the triangular lattice. Using quantum Monte Carlo (QMC) numerics, we map out the phase diagram of this model at half-filling. At  $T = 0$ , we show that this model exhibits a superfluid phase at small  $V/t$  and an insulating phase at large  $V/t$ , separated by a continuous quantum phase transition at  $V_c/t \approx 19.8$ . The insulating phase at  $T = 0$  appears to have no conventional broken symmetries, and is thus a uniform Mott insulator (a ‘spin liquid’ in magnetic language). We characterize this insulating phase as a uniform  $Z_2$  fractionalized insulator from the topological order in the ground state and estimate its vison gap. Consistent with this identification, there is no apparent thermal phase transition upon heating the insulator. The insulating phase instead smoothly crosses over into the high temperature paramagnet via an intermediate cooperative paramagnetic regime. We also study the superfluid-to-normal thermal transition for  $V < V_c$ . We find that this is a Kosterlitz-Thouless transition at small  $V/t$  but changes to a first order transition for  $V$  closer to  $V_c$ . We argue that this first order thermal transition is consistent with the presence of a nearby  $Z_2$  insulating ground state obtained from the superfluid ground state by condensing double vortices.

PACS numbers: 75.10.Jm, 05.30.Jp, 71.27.+a, 75.40.Mg

## I. INTRODUCTION

Spin liquids are quantum disordered paramagnetic phases that preserve all lattice symmetries. While there has been considerable progress in understanding the effective field theories and properties of such spin liquid phases<sup>1,2,3,4,5,6</sup>, showing that the excitations in this phase carry fractional quantum numbers and interact with emergent gauge fields, there are very few microscopic models which can be convincingly shown to exhibit a spin liquid phase and they fall, roughly, into two categories. One class of microscopic Hamiltonians are quantum dimer models<sup>7,8</sup>, which have been proposed to describe spin gapped phases of quantum magnets. Some of these models, on the triangular and kagome lattice in two dimensions, exhibit  $Z_2$  fractionalized quantum disordered phases. However, the Hilbert space of such quantum dimer models has a strong local constraint, namely, the number of dimers emerging from a site is fixed. It is therefore interesting to examine other models which do not have such local Hilbert space constraints and, thus, no extra conservation laws other than the total spin or total  $S_z$ . Under this second category are models, which incorporate a so-called ‘cluster charging’ energy<sup>9</sup>, which penalizes spin configurations where  $S_z$  summed over a local ‘cluster’ of sites differs significantly from its mean value. Some simple models of this type can be shown to reduce to effective quantum dimer Hamiltonians in the limit of a large charging energy, with the Hilbert space constraints emerging at low energy from energetic considerations. By the usual mapping between  $S = 1/2$  spins and hard core bosons, such quantum spin models can be alternatively viewed as boson models. The spin liq-

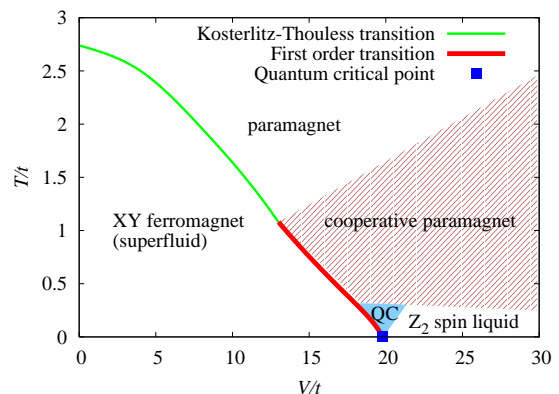


FIG. 1: (color online). The schematic phase diagram of the model given by Eq.(1) or equivalently Eq.(2). The superfluid-insulator transition in the model (1) corresponds to the XY ferromagnet to spin liquid transition in the model (2). Notice that the  $Z_2$  fractionalized Mott insulator ( $Z_2$  spin liquid) exists only at zero temperature in two dimensions and as a consequence, there is no finite temperature phase transition in the paramagnetic region, but only the crossover between different regimes as explained in the text. Near the quantum critical point between the superfluid and the  $Z_2$  fractionalized insulator, there should be a quantum critical region (denoted as QC in the figure) that is not discussed in the present paper.

uid phase of the spin model at zero magnetization then corresponds to a uniform Mott insulator of bosons at half-filling.

In this paper we study, using a generalized stochastic series expansion QMC algorithm<sup>10,11</sup>, a ‘cluster charging’ model of hard core bosons on the kagome lattice

with the Hamiltonian

$$H_b = -t \sum_{(i,j)} (b_i^\dagger b_j + \text{H.c.}) + V \sum_{\square} (n_{\square})^2 - \mu \sum_i n_i. \quad (1)$$

Here  $b_i^\dagger (b_j)$  is the boson creation(annihilation) operator,  $t > 0$  is the hopping amplitude,  $V > 0$  is the repulsion strength,  $n_i = b_i^\dagger b_i$  is the number operator, and  $\mu = 12V$  is the chemical potential which fixes the boson density to be at half-filling. The hopping term connects only the first, second and third neighbors. The repulsive interaction is similarly short-ranged. The main result of this paper is the phase diagram summarized in Fig. (1).

We begin by reviewing our earlier results<sup>12</sup> which show that model (1) exhibits, at  $T = 0$ , a superfluid-insulator quantum phase transition at  $(V/t)_c \approx 19.8$ . The insulating phase is a uniform, topologically ordered,  $Z_2$  Mott insulator. We then present new results for the finite temperature phase diagram. We find that the insulator crosses over into the high temperature normal phase via a cooperative fluctuation regime but with apparently no intervening thermal phase transitions. This bolsters the case for no broken lattice symmetries in the insulating phase. On the superfluid side, for small values of  $V/t$ , raising temperature leads to a Kosterlitz-Thouless (KT) transition from the superfluid phase to a normal phase. As we approach the quantum critical point however, with  $V/t \gtrsim 13$ , the KT transition converts into a first order transition. We argue, from a renormalization group analysis of an appropriate sine Gordon model, that this is consistent with an underlying quantum phase transition into a  $Z_2$  insulating phase driven by double vortex condensation.

Our model in Eq.(1) is inspired by an XXZ spin model for  $S = 1/2$  quantum spins proposed by Balents, Fisher and Girvin<sup>13</sup> (BFG), with a Hamiltonian

$$H_{\text{XXZ}} = -J_{\perp} \sum_{\square} [(S_{\square}^x)^2 + (S_{\square}^y)^2 - 3] + J_z \sum_{\square} (S_{\square}^z)^2. \quad (2)$$

Here  $S_{\square}^a = \sum_{i \in \square} S_i^a$  is a sum over the six spins on each hexagon of the kagome lattice unit cell,  $\sum_{\square}$  denotes a sum over all hexagons on the lattice. This model is easily seen to be a short-range anisotropic XXZ model, with only the first, second and third neighbor interactions being nonzero and equal to each other.

Analyzing the model in Eq.(2) for  $J_{\perp} < 0$  and  $J_z/|J_{\perp}| \gg 1$ , and interpreting each up-spin as a dimer on a triangular lattice, BFG showed<sup>13</sup> that the Hamiltonian is dual to an effective triangular lattice quantum dimer model with three dimers touching each site. In spin language, this effective model takes the form of a ring-exchange model, with an exchange scale  $J_{\text{ring}} = J_{\perp}^2/J_z$ , which describes quantum dynamics in the Hilbert space with  $S_{\square}^z = 0$  on each hexagon, the local constraint arising from energetic considerations at large  $J_z/J_{\perp}$ . Supplementing this model with an additional four-site (Rokhsar-Kivelson (RK)<sup>14</sup>) potential term of strength  $v_4$

they showed that this modified Hamiltonian is in spin liquid phase for  $v_4 = J_{\text{ring}}$ , which was argued to be stable for small deviations  $v_4 < J_{\text{ring}}$ . Later exact diagonalization (ED) numerics<sup>15</sup> showed that the ring-exchange model appears to be in this spin-liquid phase down to  $v_4 = 0$ , but only system sizes upto 20 unit cells could be explored.

The relation of the XXZ model to the hard core boson model we study follows upon using the standard mapping between  $S = 1/2$  quantum spins and hard core bosons. Specifically, the Hamiltonian we study in this paper at half-filling is equivalent to that in Eq. (2) if we set  $J_{\perp} = t > 0$  and  $J_z = V > 0$ . Since the ring-exchange physics is independent of the sign of  $J_{\perp}$ , we expect to recover, for large values of  $J_z$ , the physics of the XXZ model with  $J_{\perp} < 0$  studied by BFG. On the technical side, the choice of  $J_{\perp} > 0$  eliminates the QMC sign problem and allows us to go significantly beyond earlier work on this class of models.

This paper is organized as follows. Section II reviews some of our earlier results and presents some new results on the zero temperature phase diagram, including a discussion of topological order in the insulator. Section III discusses the finite temperature region of the insulating phase, including the temperature dependence of the energy and an estimate of the vison gap. Section III discusses numerical and analytical results for the finite temperature superfluid-normal phase transition. Section IV presents a summary of the results.

## II. ZERO TEMPERATURE PHASE DIAGRAM

We begin by reviewing the zero temperature phase diagram of model (1) which was studied by us in an earlier paper<sup>12</sup>. For  $V/t = 0$ , the bosons only experience the hard-core constraint, and therefore condense into a superfluid phase. As we turn on interactions, the local charging energy  $V$  penalizes those configurations where the total number of bosons on any hexagon deviates from its mean value of  $\bar{n}_{\square} = 3$ . At large  $V/t$ , this cluster charging energy leads to locally incompressible hexagons. This suppresses off-diagonal long range order (and superfluidity) and drives the system into an insulating phase. In the following subsections we review our earlier numerical results which show that the superfluid insulator transition is a continuous quantum phase transition with  $z = 1$ . We also review our results and present new numerical data which show that the insulator has four degenerate, topologically distinct, ground states.

### A. Quantum superfluid-insulator phase transition

For small values of  $V/t$ , we expect the ground state of model (1) to be a superfluid. We characterize this superfluid phase by its superfluid density  $\rho_s$  measured through winding number fluctuations<sup>16</sup>  $W_{a,1,2}$  in each of

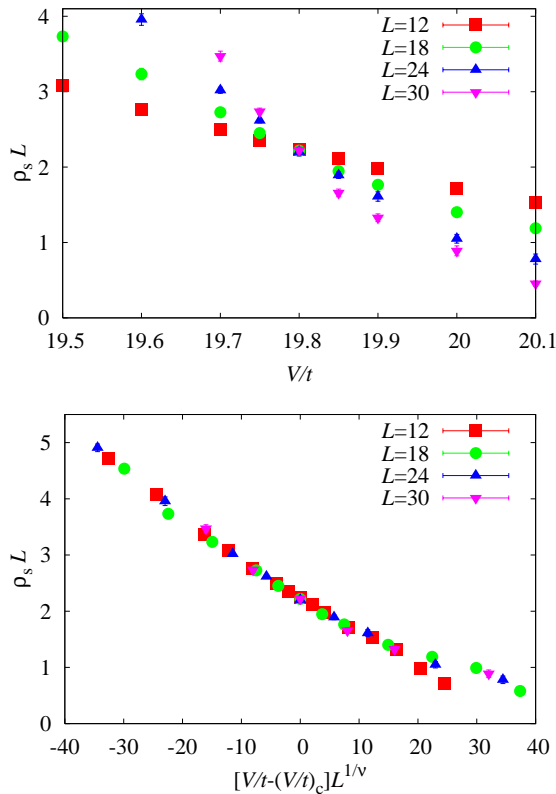


FIG. 2: (color online). Upper panel: Finite size scaling of  $\rho_s$  for  $\beta/L = 3/(4t)$ . Lower panel: Data collapse of the superfluid density  $\rho_s$  for  $\beta/L = 3/(4t)$ ,  $(V/t)_c = 19.80(2)$ , and  $\nu = 0.67(5)$ .

the two lattice directions, with

$$\rho_s = \frac{\langle W_{a_1}^2 \rangle + \langle W_{a_2}^2 \rangle}{2\beta t},$$

where  $\beta$  is the inverse temperature. For small  $V/t$ ,  $\rho_s$  is large and its value agrees with the mean field estimate obtained by Gutzwiller projecting a free Bose condensate so as to satisfy the hard core constraint<sup>17</sup>.  $\rho_s$  decreases with increasing  $V/t$ , eventually vanishing for  $V/t \gtrsim 20$  suggesting a phase transition to an insulating phase ( $\mathcal{I}^*$ ). This behavior is in sharp contrast to a nearly identical kagome lattice model where the hopping and repulsive interactions are restricted to the nearest neighbor only — in that case,<sup>18</sup> a uniform superfluid persists for arbitrarily large  $V/t$ . The absence of a jump in  $\rho_s$  on going through the transition suggests that the  $\mathcal{SF} - \mathcal{I}^*$  transition is continuous.

In the vicinity of a continuous QPT, the superfluid density should scale as

$$\rho_s = L^{-z} F_{\rho_s}(L^{1/\nu}(K_c - K), \beta/L^z), \quad (3)$$

where  $F_{\rho_s}$  is the scaling function,  $L$  is the linear system size,  $z$  the dynamical critical exponent,  $\nu$  the correlation length exponent, and  $(K_c - K) \propto (V_c - V)/t$  is the distance to the critical point. Thus if we plot  $\rho_s L^z$  as a

function of  $V/t$  at fixed aspect ratio  $\beta/L^z$ , the curves for different system sizes should intersect at the critical point. The inset of Fig. 2 shows such a plot for  $z = 1$  and  $\beta/L = 3/(4t)$  with a clear crossing point at  $(V/t)_c \approx 19.8$ . The data is thus consistent with a continuous  $\mathcal{SF} - \mathcal{I}^*$  transition with the dynamical exponent  $z = 1$ . To obtain the correlation length exponent  $\nu$ , we plot  $\rho_s L$  as a function of  $[(V/t)_c - V/t]L^{1/\nu}$  for different system sizes. It follows from Eq. (3) that the curves for different system sizes should collapse onto a universal curve  $F_{\rho_s}$  for a properly chosen  $(V/t)_c$  and  $\nu$ . In Fig. 2, we show such a data collapse for  $(V/t)_c = 19.80(2)$  and  $\nu = 0.67(5)$ . The error bars are estimated from the stability of the collapse towards varying the parameters. To summarize, we find a continuous  $\mathcal{SF} - \mathcal{I}^*$  transition with exponents  $z = 1$  and  $\nu = 0.67(5)$ . We next examine the nature of the insulator  $\mathcal{I}^*$ .

## B. Characterizing $\mathcal{I}^*$ : Topological degeneracy and absence of broken symmetries

In order to test whether the insulating phase of this model is a conventional broken symmetry state, we have studied correlation functions in  $\mathcal{I}^*$ . We have looked for signatures of diagonal (density), bond or plaquette ordering by studying the equal-time density and bond structure factors to check for different ordering patterns. Even for system sizes as large as  $48 \times 48$  kagome unit cells and temperatures as low as  $T/J_{\text{ring}} \approx 0.2$ , where  $J_{\text{ring}} = t^2/V$ , we find no evidence of any Bragg peaks, or any ordering tendency, in these correlators. This appears to rule out the possibility that  $\mathcal{I}^*$  is a conventional lattice symmetry broken state. Additional evidence for a uniform insulating phase comes from the fact that if the insulator had broken lattice symmetries it would not be smoothly connected to the high temperature paramagnet but be necessarily be separated from it by a thermal phase transition. However, we find no apparent signs of any thermal phase transition upon heating up from  $T = 0$  towards the uncorrelated high  $T$  paramagnet.

For a system of bosons, momentum counting arguments<sup>19,20</sup> show that an insulating state at half-filling could either be a conventional state with broken lattice symmetries or must *necessarily* have topological order which means the ground state degeneracy depends on the topology of the system. Since we have ruled out, as best as we can, the possibility that the insulating phase breaks lattice symmetries, we next examine the insulating phase for signs of topological order.

On a lattice with periodic boundary conditions in both lattice directions, the subspace of configurations with  $n_{\square} = 3$  on every hexagon of the kagome lattice is identical to the Hilbert space of a triangular lattice quantum dimer model, with three dimers touching each site (identifying the hardcore boson with a dimer). It is well known that such quantum dimer models have well defined topological sectors, distinguished by the eigenvalues of a

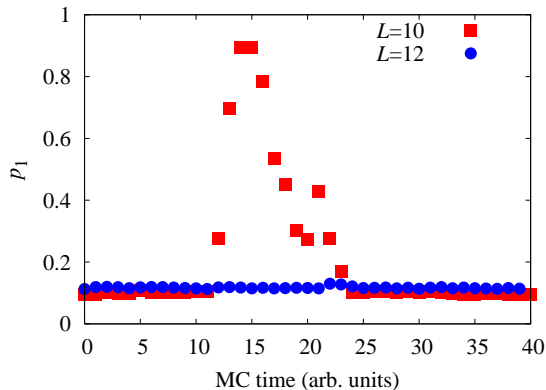


FIG. 3: (color online). Average parities as a function of Monte Carlo time for two different system sizes and  $T = t/20$  in the insulator at  $V/t = 24$ . The start configuration has  $p_{1,2} = 0$ . The parities are finite because there is a small density of defects. The parities for  $L = 12$  do not fluctuate indicating that the system does not change its topological sector whereas they strongly fluctuate for  $L = 10$  indicating that the topological sector is changing.

nonlocal operator, which do not mix under the dynamics generated by the Hamiltonian. In the context of our model, if we set  $t/V = 0$  and examine the classical ground states, which do respect  $n_{\square} = 3$ , these sectors correspond to having, for each lattice direction  $a_{1,2}$ , an odd (or even) number of bosons on each row (or column) of the lattice (so called “parity sectors”). The row/column parities defined in this manner *do not*, however, specify topological sectors of model (1) since for any nonzero  $t$ , no matter how small, there will be a small density of defect hexagons<sup>21</sup> with  $n_{\square} \neq 3$  so that the row or column parity is not conserved under the Hamiltonian dynamics. How do we then look for topological sectors in the ground state of model (1)?

We have checked in our QMC numerics, that if we start from a configuration which lies in the dimer subspace with a certain row/column parity, then the QMC algorithm generates a small density of particle-hole pair defects in equilibrium, so that the quantum ground state no longer lies in the “dimer subspace”. However, for a large enough linear system size  $L$  at a given value of  $V/t$  (e.g.,  $L \gtrsim 10$  at  $V/t = 26$ ), our simulations with the longest accessible MC steps do not lead to *any* nonlocal boson moves which wind around the lattice, see Fig. 3. Thus the winding number identically vanishes, and each configuration in the simulation which lies in the dimer subspace belongs to the same parity sector as the initial configuration. The full ground state accessed by the QMC is, in this sense, perturbatively connected to the initial parity sector. In other words, we can start with the equilibrium QMC ground state and erase nearby particle-hole defects in pairs and obtain a state which lies entirely in the starting topological sector. It is in this sense that we can identify the four topological sectors even for model (1), and we can continue to label them

simply by the row/column parity of that component of the ground state wavefunction which lies in the dimer subspace. The four ground state wavefunctions can be thus be written as

$$\begin{aligned} |\psi_{00}\rangle &= |\psi_{00}^d\rangle + |\psi'_{00}\rangle, \\ |\psi_{01}\rangle &= |\psi_{01}^d\rangle + |\psi'_{01}\rangle, \\ |\psi_{10}\rangle &= |\psi_{10}^d\rangle + |\psi'_{10}\rangle, \\ |\psi_{11}\rangle &= |\psi_{11}^d\rangle + |\psi'_{11}\rangle, \end{aligned}$$

where  $|\psi_{ab}^d\rangle$  denote the components of the wavefunctions that lie in the dimer subspace defined by parities  $a$  and  $b$  and  $|\psi'_{ab}\rangle$  denote the components of the wavefunctions that do not lie in the dimer subspace but are connected to  $|\psi_{ab}\rangle$  by short range hops of the bosons. It is clear that these wavefunctions are distinct eigenstates of our local Hamiltonian and they are not connected by local moves. For a *topologically ordered* insulator, the ground state energy should be *identical* in each of the four topological sectors (on a torus) leading to a ground state degeneracy of four. We have computed the energy of the four ground states by starting our simulations from configurations in the dimer subspace lying in four different parity sectors. We find that they are equal within statistical errors, which is strong evidence for topological order<sup>22</sup>.

### C. Vison correlations

A second signature of  $Z_2$  fractionalization is that visons, which are gapped  $Z_2$  vortices in the effective field theory description, should have exponentially decaying spatial correlations. The spatial vison-vison correlation function is the expectation value of a string operator in terms of the spins. For the ring-exchange model (valid for  $V/t \rightarrow \infty$ ), it takes the form<sup>13</sup>:

$$C_{\text{vv}}(r_{ij}) = |\langle 0 | \prod_{k=i}^j e^{i\pi n_k} | 0 \rangle|, \quad (4)$$

where  $|0\rangle$  denotes the ground state and the product is along some path on the kagome lattice that contains an even number of sites, starts at site  $i$ , and ends at site  $j$ , making only “ $\pm 60^\circ$ ” turns to the left or right.  $n_k = 0, 1$  is the number of bosons at site  $k$ . The absolute value of the product in Eq. (4) is *path-independent* in the dimer subspace, and it is expected to decay exponentially in the topologically ordered phase. In model (1) at finite  $V/t$ , ground state no longer lies entirely in the dimer subspace, but will mix in configurations with particle-hole defects. However, in the same manner as we have used the dimer subspace component of the wavefunction to define topological sectors, we can similarly use that wavefunction component to also compute the vison correlator. We have found that  $C_{\text{vv}}(r_{ij})$ , computed by essentially dropping all configurations containing particle-hole

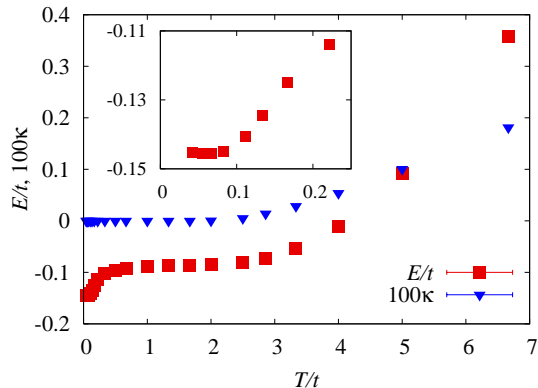


FIG. 4: (color online). Energy per site  $E$  and compressibility  $\kappa$  versus temperature for  $L = 24$  ( $V/t=20.5$ ). The energy rises exponentially at very low  $T$  (see inset) with a wide intermediate plateau from  $T/t \sim 0.5-3$  (see text). The compressibility is zero (within error bar) at low  $T$ , rising only at  $T \sim 2.5t$  once gapped charge (spinon) excitations become relevant.

defects, decays exponentially in  $\mathcal{I}^*$ , again signaling topological order in  $\mathcal{I}^*$ . At  $V/t = 20.5$ , we estimate a “decay length”,  $\xi = 1.43(5)$ , which is comparable to its value at the RK point of the ring-exchange model<sup>13</sup>,  $\xi \approx 1$ , and to that found by ED<sup>15</sup>,  $\xi \approx 1.7$ , in the ring-exchange model with  $v_4 = 0$ . This exponential decay shows us that significant local particle rearrangements and fluctuations are possible even in the insulating phase — such fluctuations are generated by the effective ring exchange dynamics of the bosons.

### III. HEATING THE INSULATOR: COOPERATIVE PARAMAGNETIC REGIME AND THE VISON GAP

To provide further evidence for gapped vison excitations, we display the temperature dependence of the system energy per site and compressibility

$$\kappa = \frac{\beta}{N} \left\langle \left( \sum_i n_i \right)^2 \right\rangle$$

in Fig. 4. Upon heating up from the ground state, the energy exhibits a two-step increase, with a distinct intermediate plateau. At the lowest temperature, the energy increases exponentially from the spin-liquid ground state as seen from the inset of Fig. 4. The energy then reaches a plateau at a temperature  $T \sim J_{\text{ring}}$ . This plateau corresponds to a regime where the system dominantly explores configurations with  $n_{\square} = 3$  on each hexagon. In spin language, it corresponds to a “cooperative paramagnet”. Upon heating further, the energy increases beyond its plateau value when the temperature becomes comparable to the local charge gap set by  $V$ . We confirm this by noting that there is a sharp increase in  $\kappa$  at this higher temperature (also shown in Fig. 4).

Heating up from  $T = 0$ , we therefore identify the lowest energy excitations out of the ground state as coming from vison-pair excitations of the spin liquid (since the charge gap is much larger). The temperature dependence of the energy thus gives us a rough idea of the single vison gap; for  $V/t = 20.5$ , we estimate  $E_v/t \sim 0.35(15)$ .

Note that the classical model with  $t = 0$  has a large entropy at  $T = 0$  arising from a macroscopic number of degenerate classical ground states. When one turns on a nonzero  $t$ , this degeneracy is lifted as the ground state becomes a quantum spin liquid which supports vison excitations ( $Z_2$  vortices). From the point of view of the spin liquid ground state, we can therefore view the large entropy density of the classical dimer state as arising from the large entropy density of multiple vison excitations as the system is heated. This means that the energy curve should have a finite temperature plateau at the energy level with the largest entropy density where, very roughly, half of all allowed visons get excited which contributes to a large configurational entropy of visons. This happens at an energy  $E_s \approx E_0/2$  as measured from zero classical ground state energy, where  $E_0$  is the quantum ground state energy. This is consistent with our numerical data.

### IV. HEATING THE SUPERFLUID: SUPERFLUID-NORMAL PHASE TRANSITION

For  $V < V_c$ , the system is in a superfluid ground state. Heating this superfluid leads to transition from a superfluid phase to a normal liquid phase at finite temperatures. This transition is usually of a Kosterlitz-Thouless (KT) type<sup>23,24</sup> that is driven by vortex unbinding. In principle, this transition can also be first order when the vortex core energy is small enough<sup>25,26</sup>. We find from our numerics that the thermal superfluid normal transition is a KT transition at small enough values of  $V/t$ . This goes along with the conventional wisdom. However, the transition becomes first order roughly at  $V/t \gtrsim 13(1)$ . This appears to be a novel example of a discontinuous thermal superfluid-normal transition in a microscopic two-dimensional quantum model.

#### A. QMC results for the SF-normal thermal transition

In Fig. 5, we show the superfluid density  $\rho_s$  and the system energy  $E$  as a function of temperature at  $V/t = 4$ . Both quantities exhibit smooth behavior. The superfluid density should be discontinuous at the KT transition with the universal jump

$$\Delta\rho_s = \frac{2T_{\text{KT}}}{\pi},$$

where  $T_{\text{KT}}$  is the KT critical temperature. However, this discontinuity is approached only logarithmically as the

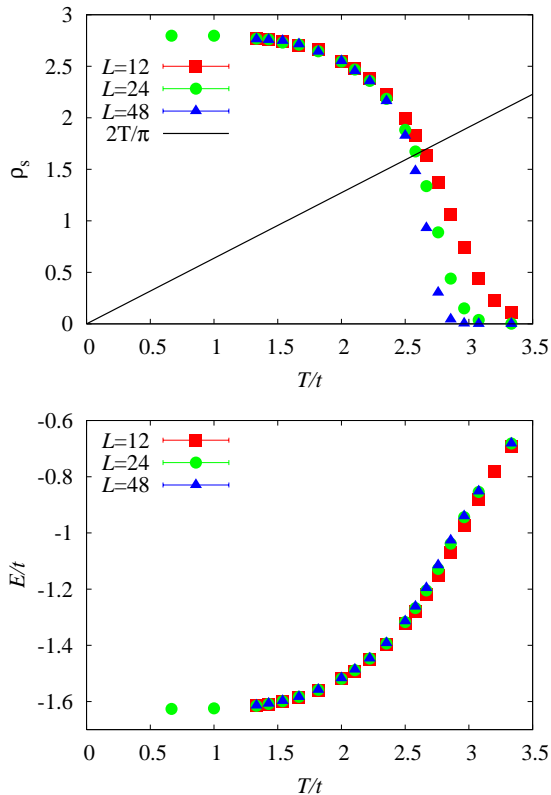


FIG. 5: (color online). The superfluid density  $\rho_s$  and the energy  $E$  as a function of temperature at  $V/t = 16$ .

system size increases. The RG equations<sup>27</sup> predict that in the vicinity of the KT transition the superfluid density scales as<sup>28,29,30</sup>

$$\rho_s = \frac{2T}{\pi} \left\{ 1 + \frac{F[(T - T_{\text{KT}}) \ln^2(L/L_0)]}{2 \ln(L/L_0)} \right\}, \quad (5)$$

where  $F$  is the scaling functions such that  $F(x) \approx 1 + O(x)$  for small values of  $x$ ,  $L$  is the linear system size, and  $L_0$  is some length scale. If one plots  $(\pi\rho_s/T - 2) \ln(L/L_0)$  as a function of  $(T - T_{\text{KT}}) \ln^2(L/L_0)$  then it follows from Eq. 5 that the curves for different system sizes should collapse onto a universal curve  $F$  for a properly chosen  $T_{\text{KT}}$  and  $L_0$ . In addition,  $(\pi\rho_s/T - 2) \ln(L/L_0)$  should take a value of 1 at the KT transition point.

In Fig. 6, we show such a data collapse for  $T_{\text{KT}} = 2.486t$  and  $L_0 = 2$ . Thus we can conclude that the transition at  $V/t = 4$  is a KT transition.

The situation is strikingly different for values of  $V/t$  roughly larger than 13. In Fig. 7, we show the superfluid density and the system energy as a function of temperature at  $V/t = 16$ . Both the superfluid density and the energy jump suggesting that the transition is first order. As can be seen from Fig. 8, the distribution of the kinetic energy,  $E_k = -t\langle(b_i^\dagger b_j + \text{H.c.})\rangle$ , close to the transition has a clearly visible double peaked structure even for very small systems sizes indicating that the transition is strongly first order. The double peaked structure

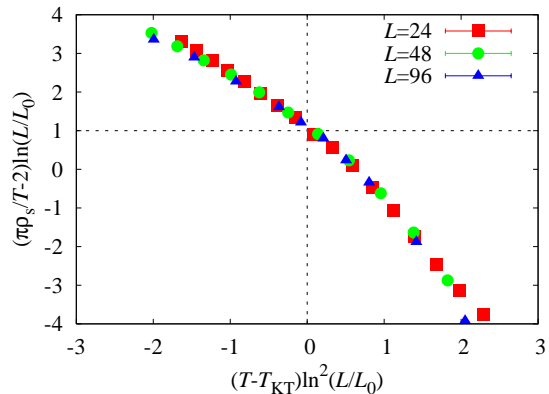


FIG. 6: (color online). Data collapse of the superfluid density  $\rho_s$  for  $T_{\text{KT}} = 2.486t$  and  $L_0 = 2$ . Horizontal and vertical dashes lines are guides for the eye.

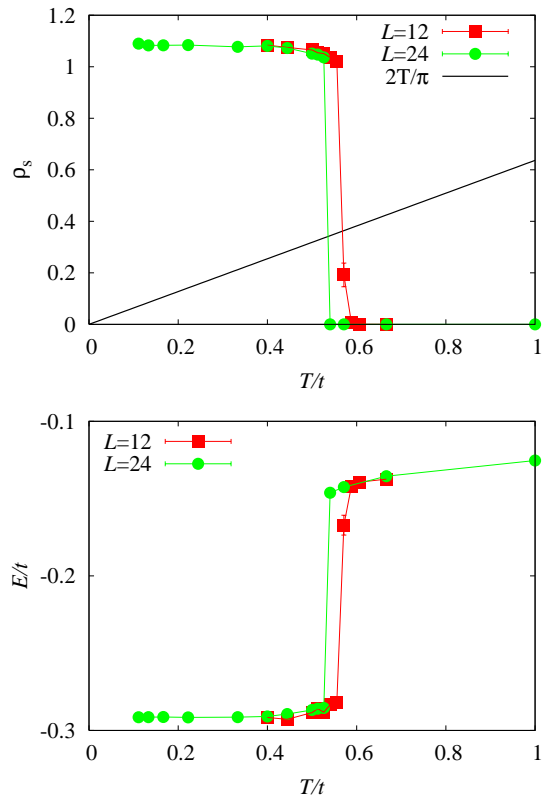


FIG. 7: (color online). The superfluid density  $\rho_s$  and the energy  $E$  as a function of temperature at  $V/t = 16$ .

becomes more pronounced, leading to two well-separated peaks, as the systems size increases. We also observe hysteresis effects by crossing the transition point upon heating or cooling the system (not shown). This is also indicates that the transition is first order.

For  $13 \lesssim V/t \lesssim 17.5$ , the normal liquid just above  $T_c$  has an energy which is nearly temperature independent for a range of temperatures. In this sense, it is analogous to the finite temperature plateau regime shown in Fig. 4

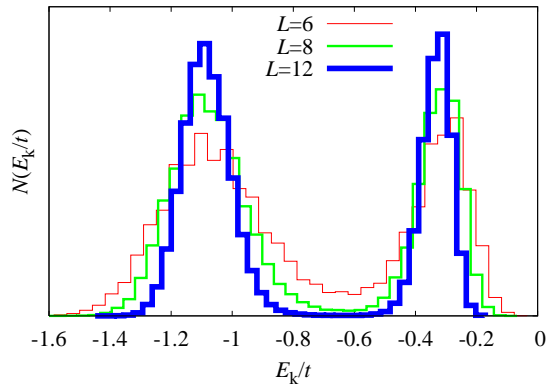


FIG. 8: (color online). Distribution of the kinetic energy close to the transition for different systems sizes and slightly different temperatures ( $\beta t = 1.67$  for  $L = 6$ ,  $\beta t = 1.745$  for  $L = 8$ , and  $\beta t = 1.77$  for  $L = 12$ ) at  $V/t = 16$ . A double peak structure is visible even for very small systems sizes and it becomes more pronounced, leading to two well-separated peaks, as the system size increases indicating a strongly first order transition.

which is obtained upon heating the insulator. This normal liquid can be well approximated by a classical liquid with  $n_{\square} = 3$  on each kagome hexagon, a so-called “cooperative paramagnet” in spin language. However, when we increase  $V/t$  in the range  $17.5 \lesssim V/t \lesssim V_c/t$ , the normal liquid just above  $T_c$  has increasingly significant quantum dynamics (as it lies in the quantum critical regime of the quantum phase transition) and, consequently, a progressively lower entropy than the classical liquid with  $n_{\square} = 3$  on each kagome hexagon. The first order thermal transition correspondingly gets weaker for  $V \rightarrow V_c$  and eventually merges into the continuous quantum phase transition at  $V_c$ .

### B. Analysis of the thermal superfluid-normal transition

We next turn to an analysis of the thermal superfluid-normal transition in order to shed some light on the observation that it becomes first order rather than a continuous Kosterlitz-Thouless transition when  $V/t$  is close to its quantum critical value. One qualitative way to understand this physics is to appeal to an entropy mismatch argument. At low  $T$  in the superfluid, the only relevant excitation is the superfluid sound mode. This has a velocity  $c_s$  which is nonsingular at the  $z = 1$  quantum phase transition into the insulator. The low temperature specific heat and entropy thus scale as  $\sim T^2/c_s$  deep in the superfluid. At large  $V/t$  the finite  $T$  normal state, if it lies in the “cooperative paramagnet” regime, is highly constrained and can be described very crudely by all possible classical configurations for which  $n_{\square} = 3$  on each hexagon of the kagome lattice. This classical picture where we ignore all quantum fluctuations then

predicts a large constant entropy  $S_{\text{cl}}$  in the normal state. Extrapolating from the low temperature superfluid state to the normal state thus leads to a large entropy mismatch,  $S_{\text{cl}} - T_c^2/c_s$ , at the transition when  $T_c$  is small. Clearly, once  $T_c$  decreases below a certain value, this entropy mismatch cannot be satisfied by the configurational entropy of a *dilute* gas of vortices. The superfluid to normal transition must, at this stage, involve producing a large number of vortices over a small temperature interval to make up for this entropy mismatch, implying a large vortex fugacity. Such a large vortex fugacity is well known to modify the KT transition into a first order transition. Of course this argument does not hold very close to the quantum critical point where the normal state just above  $T_c$  is not a simple classical liquid with an entropy  $S_{\text{cl}}$ , but is instead a quantum critical liquid.

In what follows, we will provide a slightly different view of the thermal transition. It is well known that a  $Z_2$  fractionalized insulating ground state can be obtained from a superfluid ground state by condensing double vortices instead of single vortices. If the superfluid is proximate to such an exotic insulating ground state, as our other results show, then the thermal excitations of such a superfluid must include low lying double vortex excitations in addition to single vortices. Our aim here will be to infer the presence of these low energy double vortices from the observed first order superfluid-normal transition. We will therefore attempt to study the thermal SF-normal transition taking into account both single and double vortices in a sine Gordon model.

### C. Phenomenological model

Our discussion will use the classical sine Gordon model to describe the thermal phase transition from the superfluid to the normal phase. To obtain this, we begin with the classical XY model written in vortex language

$$\beta H_v = 2\pi^2 K \sum_{\mathbf{r}\mathbf{r}'} n_{\mathbf{r}} n_{\mathbf{r}'} G(\mathbf{r} - \mathbf{r}') + \sum_{\mathbf{r}} \beta E_c(n_{\mathbf{r}}) \quad (6)$$

where  $n_{\mathbf{r}}$  is the vortex number,  $G(\mathbf{r} - \mathbf{r}')$  is the vortex interaction (which is logarithmic at large distances),  $K$  is the superfluid stiffness normalized by the temperature, and  $E_c(n_{\mathbf{r}})$  is the local core energy of a vortex with vorticity  $n_{\mathbf{r}}$ . We expect that at a fixed temperature  $T$ , the normalized stiffness  $K$  will decrease as we increase  $V/t$ . The hope is that such a classical description is adequate to qualitatively capture the physics of the thermal transition with quantum fluctuations being important in fixing the parameters of this classical vortex Hamiltonian.

We can go to  $\mathbf{k}$ -space where the vortex interaction takes the simple form  $G(\mathbf{k}) = 1/(4 - 2 \cos k_x - 2 \cos k_y)$  for a 2D square lattice. Actually, the only important thing is that  $G(\mathbf{k} \rightarrow 0) = 1/\mathbf{k}^2$ . The detailed form and the lattice geometry are unimportant. We can then do a Hubbard-Stratonovitch decoupling of the vortex interaction term,

writing

$$e^{-\sum_{\mathbf{k}} 2\pi^2 K n_{\mathbf{k}} n_{-\mathbf{k}} G(\mathbf{k})} \quad (7)$$

$$\sim \int D\phi_{\mathbf{k}} \phi_{\mathbf{k}}^* e^{-\sum_{\mathbf{k}} \frac{|\phi_{\mathbf{k}}|^2}{8\pi^2 K G(\mathbf{k})} + i \sum_{\mathbf{k}} \phi_{\mathbf{k}} n_{-\mathbf{k}}} \quad (8)$$

so that the partition function takes the form

$$Z \sim \int D\phi_{\mathbf{r}} \sum_{\{n_{\mathbf{r}}\}} e^{-\sum_{\langle \mathbf{r}\mathbf{r}' \rangle} (\phi_{\mathbf{r}} - \phi_{\mathbf{r}'})^2 / (8\pi^2 K) + i \sum_{\mathbf{r}} \phi_{\mathbf{r}} n_{\mathbf{r}}} \quad (9)$$

$$\times e^{-\sum_{\mathbf{r}} \beta E_c(n_{\mathbf{r}})} \quad (10)$$

Let us assign core energies  $\beta E_c(0) = 0$ ,  $\beta E_c(1) = e_1$ ,  $\beta E_c(2) = e_2$  and  $\beta E_c(n > 2) = \infty$  to simplify the situation. In that case, doing the sum over  $n_{\mathbf{r}}$  at each site leads to

$$Z \sim \int D\phi_{\mathbf{r}} e^{-\sum_{\langle \mathbf{r}\mathbf{r}' \rangle} (\phi_{\mathbf{r}} - \phi_{\mathbf{r}'})^2 / (8\pi^2 K)} \quad (11)$$

$$\times \prod_{\mathbf{r}} (1 + v_1 \cos \phi_{\mathbf{r}} + v_2 \cos 2\phi_{\mathbf{r}}). \quad (12)$$

where  $v_p = 2e^{-e_p}$ . For small  $v_p$ , we can re-exponentiate the cosine terms to get

$$Z \sim \int D\phi_{\mathbf{r}} e^{-\sum_{\langle \mathbf{r}\mathbf{r}' \rangle} (\phi_{\mathbf{r}} - \phi_{\mathbf{r}'})^2 / (8\pi^2 K)} \quad (13)$$

$$\times e^{\sum_{\mathbf{r}} (v_1 \cos \phi_{\mathbf{r}} + v_2 \cos 2\phi_{\mathbf{r}})}. \quad (14)$$

Relabelling  $1/(8\pi^2 K) \rightarrow g/2$ , and in the continuum,

$$Z_{SG} = \int D\phi_{\mathbf{r}} e^{-\int d^2\mathbf{r} [\frac{g}{2} (\nabla\phi)^2 - v_1 \cos \phi - v_2 \cos 2\phi]}. \quad (15)$$

The usual XY model corresponds to setting  $e_2 = \infty$ , or  $v_2 = 0$ . Let us refer to these sine-Gordon models as  $SG_2$  (with  $v_2 \neq 0$ , containing double vortices in addition to single vortices) and  $SG_1$  (with  $v_2 = 0$ , with just single vortices). We can now study the RG flow equations for  $SG_2$ , looking at the combined flow of  $g, v_1, v_2$ . In terms of dimensionful quantities, which will be of use later while trying to understand the numerical phase diagram, we have  $K = \rho_s/T$  ( $\rho_s$  being the superfluid stiffness), so that  $g = T/(4\pi^2\rho_s)$  and  $v_n = 2\exp[-\beta E_c(n)]$ .

#### D. RG equations

The RG begins by writing  $\phi = \phi_{>} + \phi_{<}$ , where  $\phi_{>}$  has Fourier modes with momenta  $\Lambda e^{-d\ell} < q < \Lambda$ , while the slow field  $\phi_{<}$  has the other Fourier components.  $\Lambda$  is the upper momentum cutoff. We fix it so that  $\pi\Lambda^2 = 4\pi^2$ , or  $\Lambda = 2\sqrt{\pi}$ . Integrating over the fast fields, we arrive at the following RG flow equations

$$\frac{dv_1}{d\ell} = v_1 \left(2 - \frac{1}{4\pi g}\right) + Av_1 v_2 \quad (16)$$

$$\frac{dv_2}{d\ell} = v_2 \left(2 - \frac{1}{\pi g}\right) - Bv_1^2 \quad (17)$$

$$\frac{dg}{d\ell} = C_1 v_1^2 + C_2 v_2^2 \quad (18)$$

where the coefficients  $A = \frac{\alpha_{1,1}(g)}{4\pi g}$ ,  $B = \frac{\alpha_{1,1}(g)}{16\pi g}$ ,  $C_1 = \frac{\alpha_{3,1}(g)}{128\pi^2 g}$ , and  $C_2 = \frac{\alpha_{3,4}(g)}{8\pi^2 g}$ . Here, we have defined

$$\alpha_{m,n}(g) = \int_1^\infty dx x^{m-\frac{n}{2\pi g}} J_0(x). \quad (19)$$

The lower limit of this integral defining  $\alpha_{m,n}(g)$  is set to unity — this reflects the short distance cutoff from the lattice spacing (which we have set to  $\sim 1/\Lambda$ ) in doing various spatial integrals in this calculation.

Physically, the second order correction in the flow equation for  $v_1$  may be viewed as arising from a single antivortex combining with a double vortex to give a single vortex. Similarly the second order correction to  $v_2$  can be viewed as arising from a double vortex splitting into two single vortices. For positive  $\alpha_{1,1}$  (which is the case as we find numerically), the effect of a nonzero  $v_2 \gg v_1$  is that it enhances  $v_1$  due to the second order coupling Eq. (16). The main observation we make is that *integrating out soft double vortices renormalizes the single vortex fugacity to be larger*.

We can simplify the above RG flow equations by working around  $g \sim 1/8\pi$ . Over a range of  $g$  near this value, we approximate  $\alpha_{1,1}(g) \approx 5.5g$ ,  $\alpha_{3,1}(g) \approx 6.5g$ , and  $\alpha_{3,4}(g) \approx 1.5g$ . Thus,  $A \approx 0.45$ ,  $B \approx 0.11$ ,  $C_1 \approx 0.005$ ,  $C_2 \approx 0.02$ . With these simplifications, we have numerically studied the above RG flow equations.

#### E. Flows for $v_1 \ll 1$ and $v_2 \ll v_1$

For initial  $v_2(0) = 0$  and  $v_1(0) \ll 1$ , we recover the Kosterlitz Thouless RG flow. Namely, there is a line of fixed points  $(v_1, v_2, g) \equiv (0, 0, g^*)$  with  $0 < g^* < 1/8\pi$ . The termination of this line of fixed points is the KT transition point at which the stiffness (normalized by the transition temperature),  $K^* = 1/(4\pi^2 g^*) = 2/\pi$ , is a universal number. Beyond this point,  $g$  flows to strong coupling, so that the superfluid stiffness  $K \rightarrow 0$ , signalling the non-superfluid phase. For a nonzero  $v_2(0) \ll v_1(0)$ , the above picture remains unchanged, i.e., the Kosterlitz-Thouless transition is unaffected by a small fugacity of double-vortices.

#### F. Flows for $v_1 \ll 1$ and $v_2 \sim 1 \gg v_1$

For large  $v_2(0)$ , we find that  $v_2(\ell)$  very quickly renormalizes to small values since it is strongly irrelevant in the superfluid phase. However, in the initial stages of the RG flow, it significantly affects the flow of  $v_1(\ell)$ . While  $v_1(\ell)$  tends to decrease due to the first order term  $(2 - 1/4\pi g)v_1$ , this decrease is partially offset by the positive contribution from the second order term which couples  $v_1$  and  $v_2$ . For our calculated couplings, in the regime where  $v_1$  is eventually irrelevant, it flows to zero more slowly for nonzero  $A$ . A comparison of the flows of

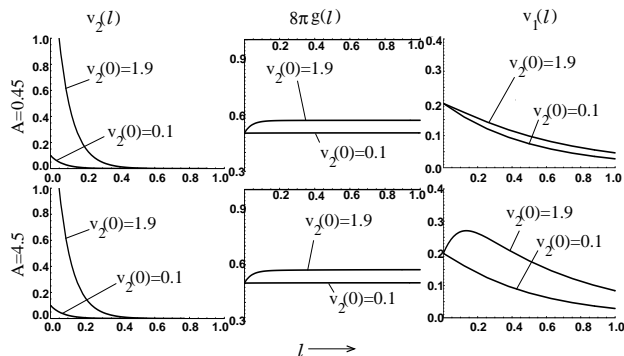


FIG. 9: Numerically computed flows for  $v_1, v_2, g$  shown for two different choices of  $v_2(0)$ . We have fixed a small  $v_1(0) = 0.2$  and  $8\pi^2g(0) = 0.5$ . The top panels shows the flows for  $A = 0.45$  in the flow equations which is the result of our perturbative calculation. The bottom panels show the flows for an artificially large  $A = 4.5$  to indicate that it leads to an enhancement of  $v_1$ .

$v_1$  and  $g$  for small and large  $v_2(0)$  is shown in the upper panel of Fig. 9.

A more striking result is obtained by artificially increasing the coefficient  $A$  in the flow equation for  $v_1$ . We find that increasing this to values larger than that given by the above perturbative calculation leads to a dramatic rise of  $v_1$  in the initial stages of the RG flow, due to coupling with  $v_2$ . This is illustrated in the lower panel of Fig. 9, where we have chosen  $A = 4.5$  instead of our calculated result  $A \approx 0.45$ . This modification of the flow equation is in a purely phenomenological spirit. Such an enhancement might be possible once we include the effect of quantum fluctuations or higher winding number vortices which we have ignored, but which do become important near the superfluid-insulator quantum phase transition; however, this is beyond the scope of our perturbative analysis.

Fig. 9 is the central qualitative result of our RG calculation. Namely, the interconversion between double vortices and single vortices together with the low core energy (a large bare fugacity) for double vortex excitations can lead to a significantly enhanced fugacity for single vortices. At the same time, the double vortices are themselves irrelevant at long length scales.

We will next use this strongly enhanced single vortex fugacity, obtained at intermediate length scales in the RG, to argue for a first order superfluid-normal thermal transition. Let us begin from the  $SG_2$  sine-Gordon theory with  $v_2(0) \gg v_1(0)$ , and follow the RG flows until we reach a fixed length scale  $\xi$  where  $v_2(\xi) \ll v_1(\xi)$ . At this stage, we can drop  $v_2$  altogether and study  $SG_1$  with only  $v_1 \neq 0$ . We have shown that at some intermediate scale,  $v_1(\xi)$  can become large. In order to accommodate this large  $v_1(\xi)$  within the  $SG_1$  theory, the  $SG_1$  action must be tuned to have a large bare fugacity for single vortices — in other words, if we ignore double vortices (which we have shown is reasonable), the large  $v_1(\xi)$  must be

viewed as arising from a large  $v_1(0)$ .

### G. Analysis of the usual sine-Gordon model

From our above RG analysis, we conclude that it makes sense to capture the effect of double vortices by studying the effect of a large bare  $v_1$  in the phase diagram of  $SG_1$ . We appeal to a variational method to study this following Ref. 31. The variational treatment for the sine-Gordon model  $SG_1$  replaces the action

$$S_{SG} = \int d^2\mathbf{r} \left[ \frac{g}{2} (\nabla\phi)^2 - v_1 \cos\phi \right] \quad (20)$$

by the variational action

$$S_0 = \int d^2\mathbf{r} \left[ \frac{\tilde{g}}{2} (\nabla\phi)^2 + \frac{1}{2} m\phi^2 \right] \quad (21)$$

with the understanding that when  $g$  gets large enough,  $v_1$  will tend to pin the field  $\phi$  to integer values leading to a mass for  $\phi$  fluctuations.

At leading order, the variational free energy

$$f_{\text{var}} \approx f_0 + \langle (S_{SG} - S_0) \rangle_0. \quad (22)$$

is minimized for a mass  $m$  which satisfies the self-consistency condition

$$\tilde{g} = g \quad (23)$$

$$m = v_1 \left( \frac{m}{m + 4\pi g} \right)^{1/8\pi g} \quad (24)$$

It is easy to show that for  $v_1 \lesssim 0.5$ , the mass is zero for  $g < g_{\text{KT}} = 1/8\pi$  while it increases continuously for  $g > 1/8\pi$ . This is the regime in which the continuous KT transition obtains in this model. At larger  $v_1 \gtrsim 0.5$ , the mass jumps discontinuously from zero to a nonzero value at a transition point  $g_c < 1/8\pi$ . This phase diagram is qualitatively illustrated in Fig. 10(b).

### H. Scenario for the SF-normal thermal transition

We now appeal to the above results to understand the thermal transition from the SF-normal thermal transition. Far from the quantum phase transition between the superfluid and the  $Z_2$  fractionalized insulator, the thermal disordering of the superfluid proceeds via the usual KT transition. As the zero temperature phase approaches the quantum critical point however, the fugacity of double vortices at finite nonzero  $T$  becomes much larger than the fugacity of single vortices since the SF- $\mathcal{I}^*$  quantum phase transition is driven by double-vortex condensation. We model this situation in our classical Hamiltonian by setting  $E_c(2) \rightarrow 0$  near the quantum phase transition, and keeping a nonzero and large  $E_c(1)$ . We expect this effective classical description to be adequate so long as we are not too close to the quantum critical point. Fig. 10(a) illustrates the expected qualitative

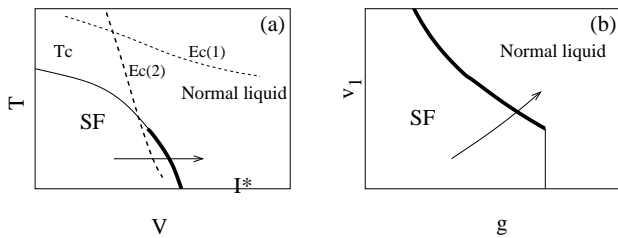


FIG. 10: (a): Assumed behavior of vortex core energies as a function of  $V/t$  in the effective classical model of vortices used to describe the thermal superfluid-normal phase transition. The solid lines are a schematic of the transition curve  $T_c(V)$  as obtained from the SSE simulations. Light solid line shows the region where this superfluid-normal transition is of the Kosterlitz Thouless type. Dark solid line indicates where the transition becomes first order. The arrow indicates a constant  $T$  trajectory going through the SF-normal transition. (b): The corresponding phase diagram in the usual sine-Gordon model. The trajectory in the left panel translates into this modified trajectory in the  $(g, v_1)$  plane.

behavior of the single and double vortex core energies, as well as  $T_c$ , as a function of  $V/t$ .

Let us imagine a trajectory at fixed temperature but along increasing  $V/t$ . In this case, the bare superfluid stiffness decreases with increasing  $V/t$ , so that  $g$  is increasing monotonically. Let us assume for simplicity that the bare single vortex core energy  $E_c(1)$  does not change with  $V/t$ . However  $E_c(2)$  rapidly drops near the quantum phase transition upon increasing  $V/t$ . From our earlier discussion the large  $v_2$  then leads to an effectively larger  $v_1$ . Thus, constant temperature trajectories in the  $(V/t, T/t)$  plane are expected to translate into trajectories depicted in Fig. 10(b) in the  $(g, v_1)$  plane. We argue that this may be responsible for the observed first order thermal transition from the superfluid to the normal

phase close to the quantum phase transition point. This first order transition must be accompanied by a nonuniversal jump in the superfluid stiffness which is larger than that predicted by KT theory. This is consistent with numerical observations presented in the previous sections.

## V. CONCLUSION

To summarize, we have studied the zero and finite temperature phase diagram of a model of hard core bosons with local interactions which exhibits a topologically ordered  $Z_2$  insulating phase at zero temperature. In magnetic language, this is equivalent to finding a quantum spin liquid phase of a  $S = 1/2$  quantum magnet. We have presented a number of numerical results, and some analytical arguments, in support of this identification. We have also studied the finite temperature phase diagram and identified a “cooperative paramagnet” regime, and seen that the superfluid to “cooperative paramagnet” transition is a first order transition rather than a BKT transition. Further work is needed to see if there is any connection between spin liquids found in simple model Hamiltonians, such as the one studied here, and the experimentally observed spin liquids in quantum magnets on kagome lattices<sup>32</sup>.

## Acknowledgments

We acknowledge support from NSERC (SVI, YBK, AP), CRC, CIAR and KRF-2005-070-C00044 (SVI, YBK), and an Alfred. P. Sloan Foundation Fellowship (AP). We thank L. Balents, R. G. Melko, and B. Seradjeh for useful discussions.

<sup>1</sup> X. G. Wen, Phys. Rev. B 44, 2664 (1991) and Cargese Lectures (1990, unpublished).  
<sup>2</sup> S. Sachdev, Phys. Rev. B 45, 12377 (1992).  
<sup>3</sup> T. Senthil and M. P. A. Fisher, Phys. Rev. B 62, 7850 (2000).  
<sup>4</sup> O. I. Motrunich and T. Senthil, Phys. Rev. B 71, 125102 (2005).  
<sup>5</sup> A. Kitaev, cond-mat/0506438 (unpublished).  
<sup>6</sup> X.-G. Wen, Phys. Rev. Lett. 90, 016803 (2003).  
<sup>7</sup> R. Moessner and S. L. Sondhi, Phys. Rev. Lett. 86, 1881 (2001).  
<sup>8</sup> G. Misguich, D. Serban and V. Pasquier, Phys. Rev. Lett. 89, 137202 (2002).  
<sup>9</sup> T. Senthil and O. I. Motrunich, Phys. Rev. B 66, 205104 (2002); Phys. Rev. Lett. 89, 277004 (2002).  
<sup>10</sup> A. W. Sandvik, Phys. Rev. B 59, R14157 (1999); O. F. Syljuåsen and A. W. Sandvik, Phys. Rev. E 66, 046701 (2002).  
<sup>11</sup> Since the standard algorithm based on a bond as the ele-

mentary lattice unit is not very efficient at large  $J_z/J_\perp$ , We use a plaquette generalization (see K. Louis and C. Gros, Phys. Rev. B 70, 100410(R) (2004)), where the elementary lattice unit is a kagome hexagon.  
<sup>12</sup> S. V. Isakov, Yong Baek Kim, and A. Paramekanti, Phys. Rev. Lett. 97, 207204 (2006).  
<sup>13</sup> L. Balents, M. P. A. Fisher, and S. M. Girvin, Phys. Rev. B 65, 224412 (2002).  
<sup>14</sup> D. S. Rokhsar and S. A. Kivelson, Phys. Rev. Lett. 61, 2376 (1988).  
<sup>15</sup> D. N. Sheng and L. Balents, Phys. Rev. Lett. 94, 146805 (2005).  
<sup>16</sup> E. L. Pollock and D.M Ceperley, Phys. Rev. B 36, 8343 (1987).  
<sup>17</sup> S. V. Isakov, A. Paramekanti, Y.-B. Kim (unpublished).  
<sup>18</sup> S. V. Isakov, S. Wessel, R. G. Melko, K. Sengupta, and Yong Baek Kim, Phys. Rev. Lett. 97, 147202 (2006).  
<sup>19</sup> M. Oshikawa, Phys. Rev. Lett. 84, 1535 (2000).  
<sup>20</sup> A. Paramekanti and A. Vishwanath, Phys. Rev. B 70,

- 245118 (2004).
- <sup>21</sup> Such defects correspond to particle-hole pairs in real space, which are necessarily bound to each other since the system is insulating and charges cannot propagate freely in the ground state.
- <sup>22</sup> For a finite size system which becomes a topologically ordered insulator in the thermodynamic limit we expect four *nearly* degenerate ground states with an energy splitting which is exponentially small in linear system size. Evaluating this splitting is beyond the scope of our simulations.
- <sup>23</sup> V. L. Berenzinskii, Zh. Eksp. Teor. Fiz. **61**, 1144 (1971) [Sov. Phys. JETP **34**, 610 (1972)].
- <sup>24</sup> J. M. Kosterlitz and D. J. Thouless, J. Phys. C **6**, 1181 (1973).
- <sup>25</sup> J. M. Caillol and D. Levesque, Phys. Rev. B **33**, 499 (1986).
- <sup>26</sup> P. Minnhagen and M. Wallin, Phys. Rev. B **36**, 5620 (1987); P. Minnhagen, Rev. Mod. Phys. **59**, 1001, (1987).
- <sup>27</sup> J. M. Kosterlitz, J. Phys. C **7**, 1046 (1974).
- <sup>28</sup> H. Weber and P. Minnhagen, Phys. Rev. B **37**, 5986 (1988).
- <sup>29</sup> P. Olsson, Phys. Rev. B **52**, 4526 (1995).
- <sup>30</sup> K. Harada and N. Kawashima, Phys. Rev. B **55**, R11949 (1997).
- <sup>31</sup> A. Diehl, M. C. Barbosa and Y. Levin, Phys. Rev. E **56**, 619 (1997).
- <sup>32</sup> J. Robert, V. Simonet, B. Canals, R. Ballou, P. Bordet, P. Lejay, and A. Stunault, Phys. Rev. Lett. **96**, 197205 (2006); J.S. Helton, K. Matan, M.P. Shores, E.A. Nytko, B.M. Bartlett, Y. Yoshida, Y. Takano, A. Suslov, Y. Qiu, J.-H. Chung, D. G. Nocera, and Y. S. Lee, Phys. Rev. Lett. **98**, 107204 (2007).